Electronic Structure of the Hydroxo and Methoxo Oxometalate Anions $MO_3(OH)^-$ and $MO_3(OCH_3)^-$ (M = Cr, Mo, and W)

Tom Waters,[†,‡] Xue-Bin Wang,[†,‡] Shenggang Li,[§] Boggavarapu Kiran,[†,‡] David A. Dixon,[§] and Lai-Sheng Wang*[,†,‡]

Department of Physics, Washington State University, 2710 University Drive, Richland, Washington 99352, W. R. Wiley Environmental Molecular Sciences Laboratory, Chemical Sciences Division, Pacific Northwest National Laboratory, P.O. Box 999, MS-K88, Richland, Washington 99352, and Chemistry Department, The University of Alabama, Shelby Hall, Box 870336, Tuscaloosa, Alabama 35487-0336

Received: August 18, 2005; In Final Form: October 13, 2005

The electronic structure of the mononuclear hydroxo $MO_3(OH)^-$ and methoxo $MO_3(OCH_3)^-$ Group 6 oxometalate anions (M = Cr, Mo, and W) were examined by photodetachment photoelectron spectroscopy and electronic structure calculations at the density functional and CCSD(T) levels of theory. All of the anions exhibited high electron binding energies (>4.9 eV), with the lowest-energy detachment features arising from oxygen 2p-based orbitals. The combined experimental and theoretical results allowed the change in molecular orbital energy levels to be investigated as a function of metal (Cr, Mo, or W) and ligand (−OH, $-OCH_3$). A number of fundamental thermodynamic properties of the anions and corresponding neutrals were predicted on the basis of the theoretical calculations. The calculations indicate high O−H bond dissociation energies for $MO_2(OR)(O-H)$ (R = H, CH_3) and $MO_3(O-H)$, consistent with their high Brønsted acidities (just below that of H_2SO_4 in the gas phase) and the high ionization energies of their conjugate base anions. This suggests that the corresponding radicals should readily abstract H atoms from organic molecules.

Introduction

The oxides of chromium, molybdenum, and tungsten are employed in a variety of catalytic reactions and are the focus of continuing investigation in the search for new or more efficient catalytic processes.[1,2] Current applications include the dehydrogenation and isomerization of alkanes,[3−5] alkene metathesis,[6−8] and the selective oxidation of alcohols to aldehydes.[9] Molybdenum oxides supported on zeolites are currently being tested as catalysts for the high-temperature oxidation of methane and higher alkanes.[10−13] The redox and acid−base properties of the oxides differ significantly as a function of metal and of oxide stoichiometry, which impacts their catalytic applications.

The details of the molecular mechanisms of many reactions occurring at oxide surfaces during catalytic processes are not well-established or understood, in large part due to the complexity of the catalyst surface and the possibility of different sites of reaction. Studies of isolated molecules, notably in the gas phase, are an alternative approach to developing a mechanistic understanding of catalysis at a molecular level, allowing reactivity trends to be identified in the absence of many complicating factors.[14−18] In addition, fundamental thermodynamic properties of small oxo−metal fragments derived from these experiments can aid in the interpretation of the reactivity of related metal oxide species on catalyst surfaces. In parallel with these gas-phase studies into reactivity, gas-phase studies using photoelectron spectroscopy (PES) provide information about the electronic and geometric structure of metal oxide species, which is also important for understanding the reactivity and catalytic function of related species.[19−22]

Metal−hydroxo M−OH and metal−alkoxo M−OR fragments are important intermediates in many catalytic processes occurring at metal oxide surfaces. For example, the oxidation of methane at molybdenum oxide surfaces is proposed to proceed by dissociation of methane to form Mo−OH and Mo−OCH_3 fragments,[23,24] and a similar methoxo−molybdenum intermediate has been proposed as the source of formaldehyde in the oxidation of methanol to formaldehyde at molybdenum oxide surfaces.[9] Metal−hydroxo sites often represent an important site of reaction at metal oxide surfaces, and the ability of oxo−metal fragments to activate C−H or O−H bonds of organic substrates and form a metal−hydroxo fragment is crucial to their catalytic function in many chemical, industrial− and biological processes.[25,26]

The present account describes an investigation into the electronic structure of a series of hydroxo− and methoxo− oxometalate anions, $MO_3(OH)^-$, and $MO_3(OCH_3)^-$ (M = Cr, Mo, and W) using PES and calculations at the density functional and molecular orbital (CCSD(T)) levels of theory. The results provide insight into important electronic and thermodynamic properties of these species. These anions can be considered as simple models for metal−hydroxo and metal−methoxo fragments present at oxide surfaces, and so a detailed understanding of their electronic and geometric structure should aid with an interpretation of their reactivity. This study is an extension of previous studies into the electronic structure of related mono- and polynuclear oxometalate anions of chromium, molybdenum, and tungsten.[19−21,27]

* Corresponding author. E-mail: ls.wang@pnl.gov.
[†] Washington State University.
[‡] Pacific Northwest National Laboratory.
[§] University of Alabama.

10.1021/jp054666x CCC: $30.25
Published on Web 12/06/2005

Experimental Details

Synthesis. The tetra-*n*-butylammonium (Bu_4N^+, Bu = *n*-butyl) salts of $[CrO_4]^{2-}$, $[MoO_4]^{2-}$, and $[WO_4]^{2-}$ were synthesized using standard literature methods.[28−30]

Electrospray Photodetachment Photoelectron Spectroscopy. The design and operation of the electrospray-PES apparatus has been described in detail,[31] and only a brief description is provided here. The hydroxo anions $[MO_3(OH)]^-$ were generated by electrospray of 10^{-3} M solutions of $(Bu_4N)_2[MO_4]$ in CH_3CN solvent. The methoxo anions $[MO_3(OCH_3)]^-$ were generated by electrospray of 10^{-3} M solutions of $(Bu_4N)_2[MO_4]$ from solvent CH_3OH. The solutions were sprayed from a 0.01-mm diameter syringe needle biased at −2.2 kV into a desolvation capillary maintained at ∼70 °C. Negative ions emerging from this capillary were transferred into a quadrupole ion-trap and accumulated for a period of 100 ms, before being passed into the extraction zone of a time-of-flight mass spectrometer. Anions of interest were mass-selected and decelerated before being intercepted by a laser beam in the detachment zone of a magnetic-bottle PES analyzer. The 193-nm (6.42 eV) and 157-nm (7.87 eV) photons from an excimer laser were used for photodetachment. Photoelectrons were collected at nearly 100% efficiency by the magnetic-bottle and analyzed in a 4-m long photoelectron time-of-flight tube. Photoelectron time-of-flight spectra were converted to kinetic energy spectra and calibrated with the known spectra of I^- and O^-. Binding energy spectra were calculated by subtracting the kinetic energy spectra from the known photon energies. The energy resolution ($\Delta E/E$) is estimated as approximately 2% (fwhm), that is, approximately 20 meV for 1-eV electrons, as measured from the spectra of I^- at 355 nm.

Theoretical Methods. Density functional theory (DFT) calculations employing the B3LYP functional[32] were carried out using the NWChem and Gaussian-03 programs.[33,34] Three-dimensional contours of the calculated molecular orbitals were generated using the Extensible Computational Chemistry Environment (Ecce) software.[35] The B3LYP calculations employed the aug-cc-pVTZ basis sets for H, C, and O and the Stuttgart quasi-relativistic pseudo-potentials and basis sets augmented with two f-type and one g-type polarization function for Cr, Mo, and W (denoted aug-cc-pVTZ/SECP(2f,g)[36−38] or the aug-cc-pVDZ basis set and the Stuttgart basis set without the additional f and g functions (denoted aug-cc-pVDZ/ SECP). If the geometries were optimized at this level, single-point calculations were done with the aug-cc-pVTZ/SECP(2f,g) basis set. Additional calculations on the hydroxo anions $MO_3(OH)^-$ (M = Mo, W) were carried out at the CCSD(T) level[39−41] using the program MOLPRO.[42] These calculations were done at the R/ UCCSD(T) level with a restricted HF set of orbitals and an unrestricted CCSD(T) for open-shell species. Geometries were optimized using the aug-cc-pVDZ/SECP basis set. Single-point energies at these optimized geometries were calculated using the aug-cc-pVTZ/SECP(2f,g) basis set. CCSD(T) calculations on the Cr-based structures were attempted but substantial issues with wave function convergence made these calculations impractical, consistent with difficulties with molecular orbital calculations on first-row transition metal species. For the bond energies and the adiabatic electron affinities, the zero-point energy (ZPE) corrections were taken from the B3LYP results except for MoO_4, MoO_4^-, WO_4, and WO_4^-, where the ZPE values were taken from calculations with the PW91 functional[43] following our previous work.[20]

Vertical detachment energy (VDE) values were calculated from the difference in energy between the parent anion and the ground state of the product neutral with its geometry fixed at that of the parent species. Differences in zero-point energy are not defined for such a process so they are not included in the VDE calculations. Changes in the vibrational energies are expected to be small, on the order of tenths of a kcalorie per mole. Theoretical predictions for the positions of VDEs for detachment from the HOMO-1, HOMO-2, etc., were estimated by adding the difference in the orbital energy between the HOMO and the deeper-lying orbitals to the VDE calculated for electron detachment from the HOMO. ADE values were calculated from the difference in energy between the optimized structures for the anion and the corresponding neutral species. At the CCSD(T) level, it was also possible to directly calculate VDEs and ADEs for detachment to the lowest-energy $^2A'$ state of the neutral radical, providing a test of the orbital energy approximation described above.

It is well established that the HOMO energy from DFT calculations is not a good approximation to the first ionization potential due to problems with the asymptotic behavior of most exchange-correlation potentials.[44] However, energy differences between the HOMO and more stable orbitals are expected to be well described by DFT methods.[45,46] Therefore, to allow for direct comparison between calculated orbital energies and experimental spectra, orbital energies have been shifted by a constant value for each species in order to align the energy of the HOMO with the calculated VDE from the B3LYP calculations (Table 4). Accordingly, orbital energies presented in Figures 4−7 were shifted by −2.26, −2.24, and −2.25 eV for $CrO_3(OH)^-$, $MoO_3(OH)^-$, and $WO_3(OH)^-$, and by −2.14, −2.14, and −2.18 eV for $CrO_3(OCH_3)^-$, $MoO_3(OCH_3)^-$, and $WO_3(OCH_3)^-$, respectively. It is interesting to note that the shift is approximately constant at 2.2 ± 0.1 eV for each of these species. Correlation diagrams giving the original orbital energies for each of $MO_3(OR)^-$ from the B3LYP calculations can be found in the Supporting Information.

Experimental Results

Photoelectron Spectroscopy of $MO_3(OH)^-$ and $MO_3(OCH_3)^-$. Photoelectron spectra of the anions $MO_3(OH)^-$ and $MO_3(OCH_3)^-$ (M = Cr, Mo, and W) at 193 and 157 nm are presented in Figures 1 and 2, respectively. The lowest-binding-energy feature in each spectrum results from electron detachment from the HOMO of the parent anion and is labeled X. The remaining features, resulting from detachment from deeper-lying molecular orbitals, are labeled A, B, C, and so forth, in order of increasing electron binding energy. ADEs and VDEs for each complex are given in Tables 1 and 2, respectively. ADEs were estimated by drawing a straight line along the leading edge of the threshold band and then adding a constant to the intersection with the binding energy axis to take into account instrumental resolution. These were determined from the 193-nm spectra for each complex. However, because of the lack of vibrational state resolution, these estimates should strictly be considered as upper limits to the true ADE. The VDE of each peak was measured from the peak maximum. In many cases, detachment features are expected to arise from multiple overlapping transitions, so the experimental VDEs should be considered as an average of these transitions.

The spectrum of $CrO_3(OH)^-$ exhibited three features between 4.6 and 5.8 eV, which are labeled X, A, and B (Figure 1a). The more intense feature at about 6.35 eV is labeled D and has a shoulder on the low-binding-energy side labeled C. The feature around 7 eV appears to arise from a sharper feature (labeled E) with a broader shoulder on the high-binding-energy side (labeled F).

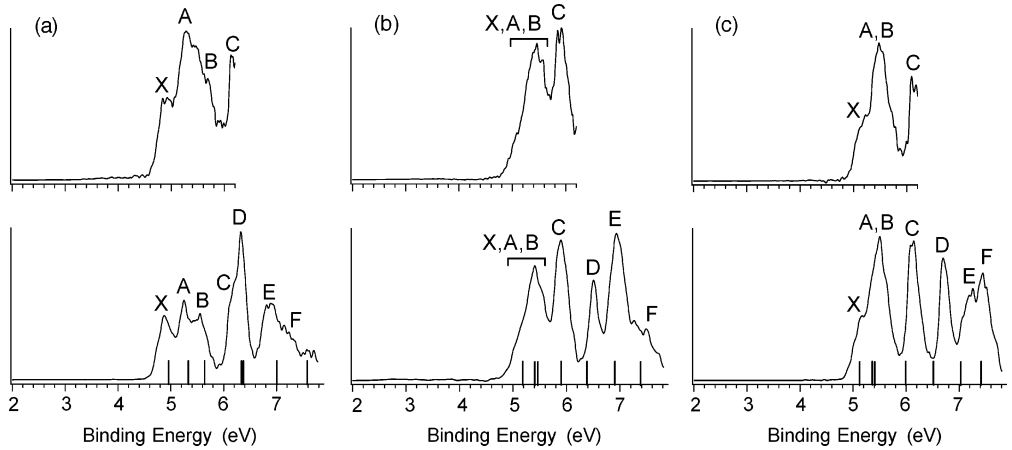

Figure 1. Photoelectron spectra of $MO_3(OH)^-$ (M = Cr, Mo, and W) at 157 nm (7.87 eV, lower) and 193 nm (6.42 eV, upper). (a) $CrO_3(OH)^-$, (b) $MoO_3(OH)^-$, and (c) $WO_3(OH)^-$. The vertical bars correspond to the positions of theoretically predicted vertical detachment energies.

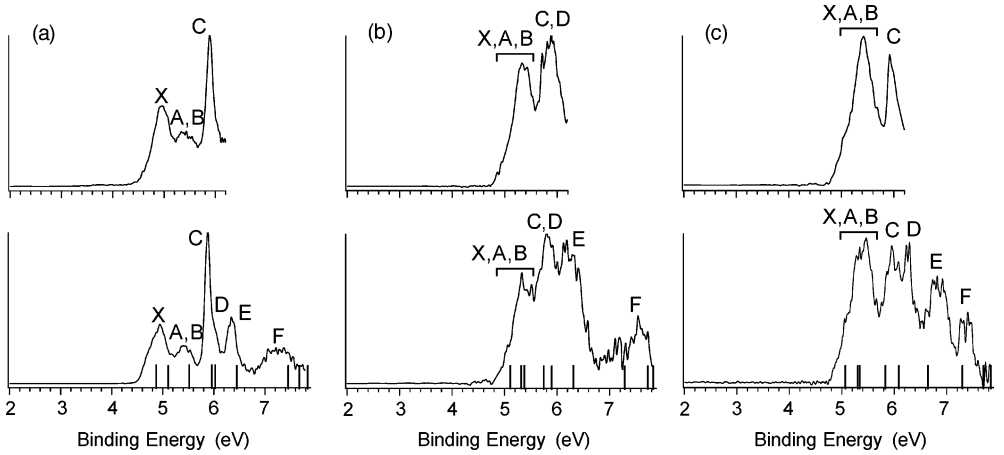

Figure 2. Photoelectron spectra of $MO_3(OCH_3)^-$ (M = Cr, Mo, and W) at 157 nm (7.87 eV, lower) and 193 nm (6.42 eV, upper). (a) $CrO_3(OCH)^-$, (b) $MoO_3(OCH)^-$, and (c) $WO_3(OCH)^-$. The vertical bars correspond to the positions of theoretically predicted vertical detachment energies.

TABLE 1: Experimental Adiabatic (ADE) and Vertical (VDE) Detachment Energies for $MO_3(OH)^-$ (M = Cr, Mo, or W)[a]

	ADE[b]	VDE						
	X	X	A	B	C	D	E	F
$CrO_3(OH)^-$	4.7(1)	4.90(5)	5.30(5)	5.50(5)	~6.2	6.35(5)	6.90(5)	~7.2
$MoO_3(OH)^-$	4.9(1)		5.2−5.6[c]		5.90(5)	6.50(5)	6.95(5)	~7.4
$WO_3(OH)^-$	5.0(1)	5.20(5)	5.50(5)[c]	5.50(5)[c]	6.15(5)	6.70(5)	7.20(5)	7.45(5)

[a] Numbers in parentheses represent the experimental uncertainties in the last digit. [b] Also represents the electron affinity of the corresponding $MO_3(OH)$ neutral species. [c] Observed bands are expected to arise from multiple transitions, so the quoted VDEs should be considered an average of these transitions.

TABLE 2: Experimental Adiabatic (ADE) and Vertical (VDE) Detachment Energies for $MO_3(OCH_3)^-$ (M = Cr, Mo, or W)[a]

	ADE[b]	VDE						
	X	X	A	B	C	D	E	F
$CrO_3(OCH_3)^-$	4.7(1)	4.95(5)	~5.40[c]	~5.40[c]	5.90(5)	6.05(5)	6.35(5)	~7.3
$MoO_3(OCH_3)^-$	4.8(1)		5.1−5.5[c]		5.8−5.9[c]	5.8−5.9[c]	~6.2	~7.5
$WO_3(OCH_3)^-$	4.9(1)		5.1−5.5[c]		5.95(5)	6.25(5)	6.85(5)	~7.4

[a] Numbers in parentheses represent the experimental uncertainties in the last digit. [b] Also represents the electron affinity of the corresponding $MO_3(OCH_3)$ neutral species. [c] Observed bands are expected to arise from multiple transitions, so the quoted VDEs should be considered an average of these transitions.

The spectra for $MoO_3(OH)^-$ and $WO_3(OH)^-$ are labeled to maintain consistency with $CrO_3(OH)^-$. The first feature observed for $MoO_3(OH)^-$ is broader than that for $CrO_3(OH)^-$ and is shifted to slightly higher binding energy (Table 1). This feature is assumed to arise from multiple detachment channels and is labeled X,A,B. The second, third, and fourth features for $MoO_3(OH)^-$ are sharper, and are labeled C, D, E, respectively. Band C is shifted to lower binding energy while band D is shifted to higher binding energy compared with the corresponding features for $CrO_3(OH)^-$ (Table 1). Bands E and F occur at similar energies for both anions, except that the feature labeled E is more intense for $MoO_3(OH)^-$ and the shoulder labeled F is more clearly resolved (Figure 1b). The spectrum of $WO_3(OH)^-$ appears very similar to that of $MoO_3(OH)^-$, as expected from previous work on MO_x^- (M = Mo, W).[20] The feature labeled A,B exhibits a shoulder on the low-binding-

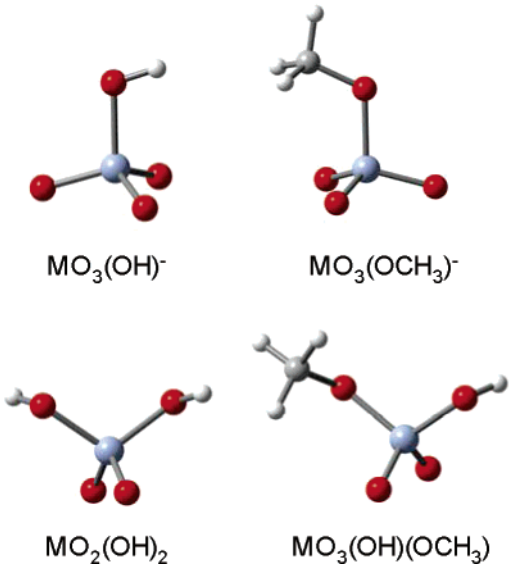

Figure 3. Calculated structures of $MO_3(OR)^-$ and $MO_2(OH)(OR)$ (M = Cr, Mo, W; R = H, CH_3).

energy side, labeled X. Features C, D, and E all occur at about 0.2−0.3 eV higher binding energy for $WO_3(OH)^-$ compared with $MoO_3(OH)^-$, while feature F occurs at a similar position for both species (Table 1).

The spectra of $CrO_3(OCH_3)^-$ (Figure 2a) are qualitatively similar to those of $CrO_3(OH)^-$, and a similar labeling scheme is used. The first two features of $CrO_3(OCH_3)^-$ are labeled X and A,B (Figure 2a). These appear similar to those for $CrO_3(OH)^-$, and their energies are largely unchanged, except that features A,B are not resolved for $CrO_3(OCH_3)^-$. The sharpest and most intense feature (labeled C) contains a shoulder on the high-binding-energy side (labeled D). The relative intensity of these features are analogous to those of C and D for $CrO_3(OH)^-$; however, their order is reversed, with the shoulder shifting from the low-binding-energy side for $CrO_3(OH)^-$ to the high-binding-energy side for $CrO_3(OCH_3)^-$ (Figures 1a, 2a). The sharper and more intense feature occurs at about 0.45 eV lower binding energy for the methoxo anion (Tables 1, 2). Similarly, feature E is shifted to about 0.55 eV lower binding energy for $CrO_3(OCH_3)^-$ (Tables 1, 2). The broad feature labeled F is more clearly resolved for $CrO_3(OCH_3)^-$ than for $CrO_3(OH)^-$ and occurs at similar binding energies for both species (Tables 1, 2).

The 157-nm spectra for $MoO_3(OCH_3)^-$ and $WO_3(OCH_3)^-$ are of poorer quality due to the weaker mass intensity of these species generated from the electrospray source (Figure 2b,c). The first features for both $MoO_3(OCH_3)^-$ and $WO_3(OCH_3)^-$ (labeled X,A,B) are broad and are again presumed to arise from multiple detachment channels as for $MoO_3(OH)^-$ and $WO_3(OH)^-$. This feature occurs at similar binding energies for both species, and it is only slightly higher than that for $CrO_3(OCH_3)^-$. The second feature labeled C,D for $MoO_3(OCH_3)^-$ is resolved into two peaks for $WO_3(OCH_3)^-$. The next feature, labeled E, occurs at similar binding energies for both $MoO_3(OCH_3)^-$ and $CrO_3(OCH_3)^-$, but at about 0.6 eV higher binding energy for $WO_3(OCH_3)^-$. The broader feature labeled F appears at similar binding energies for each of $MO_3(OCH_3)^-$ (Table 2).

Theoretical Results

Structures of $MO_3(OH)^-$ and $MO_3(OCH_3)^-$. The geometries of $MO_3(OH)^-$ and $MO_3(OCH_3)^-$ were optimized under C_s point group symmetry (Figure 3). Other conformers involving rotation of the hydroxo/methoxo ligand and/or rotation of the methyl group were predicted to be only slightly higher in energy (~0.5−1.0 kcal mol^{-1}), indicating that a range of conformers are likely to be populated in the present experiments. The electronic structures of these conformers do not differ significantly, so their presence should not change the fundamental interpretation of the PES results. Critical bond distances and angles for the anions $MO_3(OR)^-$ and neutrals $MO_3(OR)$ and $MO_2(OH)_2$ are given in Table 3. The geometries of $MO_3(OH)^-$ and $MO_3(OCH_3)^-$ suggest they can be described as OH^- or OCH_3^- coordinated to neutral MO_3. The M−OH bond distances in the anions are significantly longer than those predicted for neutral $MO_2(OH)_2$, while the MOH bond angle in the anion is smaller than that in $MO_2(OH)_2$ (Table 3). For example, the WOH bond angle in $WO_2(OH)_2$ is near 120°, substantially larger than −HOH in H_2O, and indicative of significant ionic character in the OH group. Deprotonation of $WO_2(OH)_2$ to the anion $WO_3(OH)^-$ results in this angle decreasing to about 113° for the remaining OH group. The M−O bond distances in the MO_3 unit of $MO_3(OR)^-$ increase slightly from those[19,20] in MO_3 due to the presence of the additional negative charge.

Calculated VDEs for $MO_3(OR)^-$. The calculated first VDEs for each of $MO_3(OH)^-$ and $MO_3(OCH_3)^-$ at the B3LYP level are given in Table 4 and are in good agreement with experiment (Tables 1, 2). In particular, the calculations reproduce the increase in detachment energy from Cr to Mo (~0.3 eV), with a much smaller change from Mo to W. The calculations also indicate that substitution of methoxo for hydroxo has little effect on electron binding energy, again consistent with the experimental observations. Calculations at the higher CCSD(T) level of theory for the Mo and W hydroxo anions are consistent with the experimental and the B3LYP results.

The higher-energy vertical detachment features were interpreted on the basis of the predicted orbital energies of the anion relative to that of the highest occupied molecular orbital (HOMO), in the spirit of Koopmans' theorem. These theoretical estimates are indicated as vertical lines on the experimental spectra to denote the location of the predicted transitions and are not intended to reflect their relative intensities (Figures 1 and 2).[45] The qualitative agreement between experiment and theory allowed for assignment of spectral features and enabled spectral shifts as a function of metal (Cr, Mo, or W) and ligand (OH, OCH_3) to be interpreted.

Calculated ADEs for $MO_3(OR)^-$ and Structures of $MO_3(OR)$. The ground-state geometries of neutral $MO_3(OR)$ were calculated to allow a theoretical prediction for the ADEs of $MO_3(OR)^-$ (Table 4). Calculated ADEs were in reasonable agreement with experiment, and the experimental difference between VDE and ADE of about 0.2−0.3 eV for each of $MO_3(OR)^-$ was reproduced by the calculations.

The B3LYP calculations predicted $^2A''$ ground states for both $CrO_3(OH)$ and $CrO_3(OCH_3)$ with one short and two long M−O bonds (e.g., $CrO_3(OH)$: 1.56 and 1.64 Å, respectively, Table 3), indicating that the unpaired electron of $CrO_3(OR)$ is delocalized over two oxo ligands. The situation for $WO_3(OH)$ and $MoO_3(OH)$ is more complex, with three stationary points identified within about 1 kcal mol^{-1}. For the case of $WO_3(OH)$, a $^2A''$ structure with two longer and one shorter W−O bonds and a second $^2A''$ structure with two shorter and one longer W−O bonds were located at almost identical energy (Table 3). However, both of these structures exhibited one imaginary frequency (an asymmetric stretch of the MO_2 group coupled to the torsion about the M−O(H) bond) and were 1 kcal mol^{-1} above a structure of lower C_1 symmetry. This C_1 structure has two shorter and one longer W−O bonds, consistent

TABLE 3: Optimized Geometry Parameters for $MO_3(OR)^-$, $MO_3(OR)$, and $MO_2(OH)(OR)$ (M = Cr, Mo, and W; R = H, CH_3)

molecule (state)	method[a]	sym/state	M=O	M−O	M−OR	−MOR
$CrO_3(OH)^-$	B3LYP	C_s, $^1A'$	1.598,1.603(×2)		1.831	108.6
$CrO_3(OH)$	B3LYP	C_s, $^2A''$	1.560	1.640(×2)	1.748	116.9
$CrO_2(OH)_2$	B3LYP	C_2, ^1A	1.557(×2)		1.754	114.7
$CrO_3(OCH_3)^-$	B3LYP	C_s, $^1A'$	1.599,1.604(×2)		1.818	117.7
$CrO_3(OCH_3)$	B3LYP	C_s, $^2A''$	1.562,1.645(×2)		1.734	122.5
$CrO_2(OH)(OCH_3)$	B3LYP	C_1, ^1A	1.560, 1.562		1.760(H)	114.7(H)
					1.737	123.1
$MoO_3(OH)^-$	B3LYP	C_s, $^1A'$	1.752,1.750(×2)		1.974	113.3
	CCSD(T)	C_s, $^1A'$	1.768,1.770(×2)		1.994	113.7
$MoO_3(OH)$	B3LYP	C_1, ^2A	1.711, 1.722	1.879	1.895	123.2
	B3LYP[b]	C_s, $^2A''$	1.716(×2)	1.879	1.891	129.2
	B3LYP[b]	C_s, $^2A''$	1.708	1.793(×2)	1.897	123.1
	CCSD(T)	C_s, $^2A''$	1.729	1.812(×2)	1.917	122.0
	CCSD(T)	C_s, $^2A'$	1.725(×2)	1.944	1.903	133.4
$MoO_2(OH)_2$	B3LYP	C_2, ^1A	1.706(×2)		1.900	121.6
$MoO_3(OCH_3)^-$	B3LYP	C_s, $^1A'$	1.751,1.753(×2)		1.960	122.8
$MoO_3(OCH_3)$	B3LYP	C_1, ^2A	1.713, 1.730	1.880	1.873	135.8
$MoO_2(OH)(OCH_3)$	B3LYP	C_1, ^1A	1.710, 1.709		1.906(H)	121.3(H)
					1.878	133.6
$WO_3(OH)^-$	B3LYP	C_s, $^1A'$	1.770,1.769(×2)		1.974	114.9
	CCSD(T)	C_s, $^1A'$	1.784,1.786(×2)		1.989	115.0
$WO_3(OH)$	B3LYP	C_1, ^2A	1.731, 1.758	1.863	1.901	125.9
	B3LYP[b]	C_s, $^2A''$	1.741(×2)	1.874	1.896	131.7
	B3LYP[b]	C_s, $^2A''$	1.731	1.806(×2)	1.903	126.0
	CCSD(T)	C_s, $^2A''$	1.749	1.824(×2)	1.920	124.5
	CCSD(T)	C_s, $^2A'$	1.744(×2)	1.952	1.907	134.4
$WO_2(OH)_2$	B3LYP	C_2, ^1A	1.727		1.906	123.8
$WO_3(OCH_3)^-$	B3LYP	C_s, $^1A'$	1.770,1.771(×2)		1.959	124.4
$WO_3(OCH_3)$	B3LYP	C_1, ^2A	1.734, 1.767	1.862	1.879	138.8
$WO_2(OH)(OCH_3)$	B3LYP	C_1, ^1A	1.731, 1.730		1.911(H)	123.4(H)
					1.883	136.7

[a] Calculations were carried out using the aug-cc-pVDZ/SECP basis sets; the geometries of MO_3 have r(MO) = 1.576, 1.723, and 1.740 Å for M = Cr, Mo, and W, respectively. [b] These structures have one imaginary frequency as described in the text.

TABLE 4: Calculated Vertical (VDE) and Adiabatic (ADE) Detachment Energies (eV) for $MO_3(OR)^-$ (M = Cr, Mo, or W) at the B3LYP and CCSD(T) Levels of Theory[a]

		Cr	Mo	W
$MO_3(OH)^-$	VDE	4.95	5.18/5.25	5.13/5.26
	ADE	4.66	4.86/4.96	4.86/4.98
$MO_3(OCH_3)^-$	VDE	4.85	5.11	5.06
	ADE	4.54	4.76	4.76

[a] Values after the "/" are the CCSD(T) values.

with the unpaired electron being more localized on a single oxo ligand (Table 3). This symmetry breaking for $MO_3(OR)$ (M = Mo, W) is due to mixing between the two low-lying $^2A''$ states, and similar behavior has previously been found in calculations on MO_4 radicals.[20]

Calculations on $MO_3(OH)$ (M = Mo, W) at the higher CCSD(T) level were carried out to investigate the relative energies of the lowest $^2A''$ and $^2A'$ states in more detail. The CCSD(T) calculations, constrained to C_s symmetry, predicted $^2A''$ ground states for both $MoO_3(OH)$ and $WO_3(OH)$ with one short and two longer M−O bonds (e.g., $MO_3(OH)$: 1.73 and 1.81(×2) Å, Table 3). This geometry is consistent with the unpaired electron being delocalized over two oxygen ligands and is equivalent to that for $CrO_3(OH)$ at the B3LYP level.

The CCSD(T) calculations predicted both $MO_3(OH)$ and $WO_3(OH)$ to have low-lying $^2A'$ excited states occurring at only 0.22 and 0.26 eV, respectively, above the $^2A''$ ground states. These $^2A'$ excited states exhibit two shorter and one longer M−O bonds (e.g., $MoO_3(OH)$: 1.73 × 2 and 1.94 Å; Table 3), consistent with the unpaired electron being localized on a single oxygen ligand. These geometries closely resemble those of the lower C_1 symmetry predicted for $MO_3(OH)$ and $WO_3(OH)$ from the B3LYP calculations.

The VDEs for detachment to the $^2A''$ ground state and the lowest-energy $^2A'$ excited state of neutral $MO_3(OH)$ were also calculated at the CCSD(T) level for both $MoO_3(OH)^-$ and $WO_3(OH)^-$. The calculated values of 5.61 and 5.62 eV, respectively, indicate a difference of 0.36 eV in both cases for vertical detachment to the lowest-energy $^2A''$ and $^2A'$ states. This is consistent with the values of 0.27 and 0.28 eV (estimated below) from the difference in orbital energy between the HOMO (a″) and the HOMO-2 (a′) of $MoO_3(OH)^-$ and $WO_3(OH)^-$, respectively, and supports the approximation of using the orbital energies for the higher states.

Discussion

Electronic Structure. The anions $MO_3(OR)^-$ can be formally considered as M^{VI} d^0 centers. Of course, there is substantial charge transfer, and the NBO charges[47] on the metals in the anions are +1.19 *e* for $CrO_3(OH)^-$, +1.18 *e* for $CrO_3(OCH_3)^-$, + 1.99 *e* for both anions of $MoO_3(OR)^-$, and + 2.29 *e* for both anions of $WO_3(OR)^-$. Thus the ionic character at the metal increases with increasing atomic number of the metal. The highest-energy occupied orbitals are expected to be largely derived from oxygen 2p atomic orbitals, with the three 2p atomic orbitals on each of the three oxo and single hydroxo (methoxo) ligands giving rise to 12 symmetry-adapted linear combinations that can then potentially mix with metal-based d orbitals and/or hydrogen (methyl)-based orbitals. The experimental and theoretical data allowed changes in the orbital energies for the series of hydroxo $MO_3(OH)^-$ and methoxo $MO_3(OCH_3)^-$ anions as a function of metal (M = Cr, Mo, or W) and ligand (OH, OCH_3) to be evaluated. The seven highest-energy occupied molecular orbitals for $CrO_3(OH)^-$ are illustrated in Figure 4. The corresponding orbitals for $MoO_3(OH)^-$ and $WO_3(OH)^-$ are

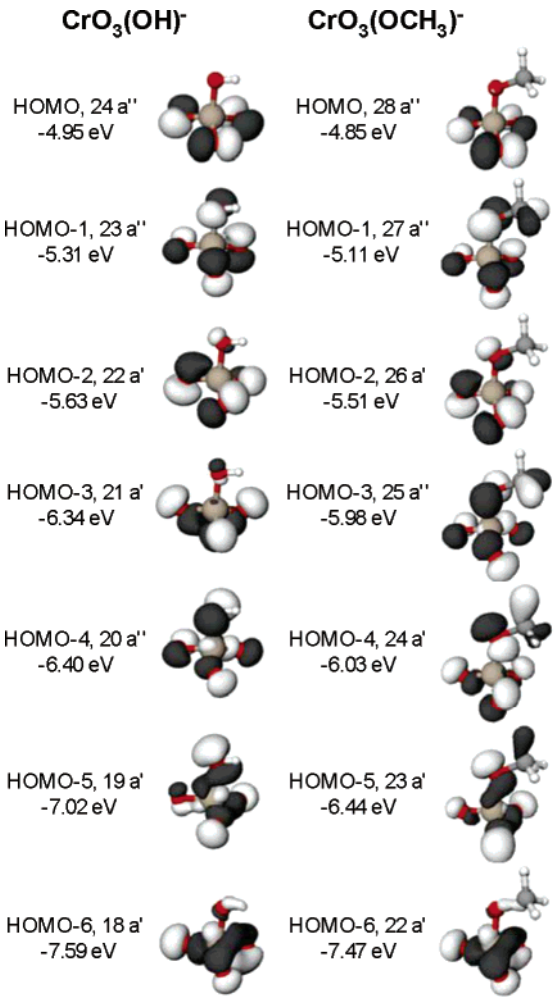

Figure 4. Molecular orbital pictures (contour cutoff 0.05 electron au^{-3}) at the B3LYP level for the seven highest-energy occupied orbitals of $CrO_3(OH)^-$ (left) and $CrO_3(OCH_3)^-$ (right). Orbital energies are from the B3LYP calculations and have been shifted for each species to align the energy of the HOMO with the calculated first VDE (see text).

qualitatively very similar. A correlation diagram relating the energies of these orbitals is presented in Figure 5.

The calculated ground-state VDE for $CrO_3(OH)^-$ is in good agreement with the experimental value of the first detachment channel (feature X; Tables 1, 4). The HOMO-1 (a″) and HOMO-2 (a′) levels of $CrO_3(OH)^-$ are more stable by 0.36 and 0.68 eV, respectively, relative to the HOMO, with detachment from these orbitals predicted to occur in the region of features A and B. The energetic separation between these orbitals is consistent with the experimental separation between features X, A, and B (Figure 1a, Table 1). Detachment from the HOMO-3 and HOMO-4 is predicted to occur at similar energies in the region of features C and D. Feature E is assigned to detachment from the HOMO-5 level, and the broad feature labeled F is assigned to detachment from the HOMO-6 level.

The experimental spectra (Figure 1) and the correlation diagram (Figure 5) allow the changes in molecular orbital energy levels of $MO_3(OH)^-$ (M = Cr, Mo, W) to be compared as a function of metal. The calculated VDEs for $MoO_3(OH)^-$ and $WO_3(OH)^-$ are both in good agreement with the experimental values. The predicted separation between the HOMO and HOMO-2 levels for $MoO_3(OH)^-$ and $WO_3(OH)^-$ is reduced to ~0.3 eV as compared to the ~0.7 eV predicted for $CrO_3(OH)^-$. This is consistent with features X, A, B appearing as a broader

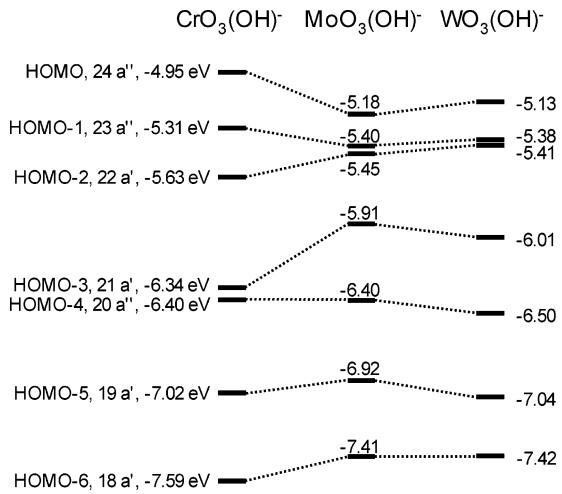

Figure 5. Correlation diagram relating the seven highest-energy occupied orbitals of $MO_3(OH)^-$ (M = Cr, Mo, or W). Orbital energies are from the B3LYP calculations and have been shifted for each species to align the energy of the HOMO with the calculated first VDE (see text).

overlapping feature for $MoO_3(OH)^-$ and $WO_3(OH)^-$, but being resolved for $CrO_3(OH)^-$ (Figure 1). The HOMO-3 and HOMO-4 levels are predicted to be almost degenerate for $CrO_3(OH)^-$, but are separated by ~0.5 eV for both $MoO_3(OH)^-$ and $WO_3(OH)^-$. This is consistent with the experimentally observed separation between bands C and D being much larger for Mo and W (~0.6 eV) as compared to Cr (~0.1 eV). The predicted detachment energies for the HOMO-3 and HOMO-4 levels of $WO_3(OH)^-$ are about 0.15 and 0.2 eV higher than the position of features C and D, respectively, indicating that these detachment energies might be underestimated for the case of $WO_3(OH)^-$ (Figure 1c). The calculated detachment energies for equivalent orbitals of $CrO_3(OH)^-$ and $MoO_3(OH)^-$ are in closer agreement with the experimental data (Figure 1a,b). The HOMO-5 and HOMO-6 levels are predicted to occur at similar energies for each of the $MO_3(OH)^-$ anions, again consistent with the experimental observations (Figure 1).

The seven highest-energy occupied orbitals for $CrO_3(OCH_3)^-$ are also illustrated in Figure 4, allowing comparison with the equivalent orbitals for $CrO_3(OH)^-$. A correlation diagram relating the energies of these orbitals is given in Figure 6. The HOMO to HOMO-2 levels of $CrO_3(OH)^-$ and $CrO_3(OCH_3)^-$ are predicted to occur at very similar energies, consistent with bands X, A, and B occurring at equivalent binding energies for both species. The HOMO-1 level is predicted to be slightly destabilized from $CrO_3(OH)^-$ to $CrO_3(OCH_3)^-$ (Figure 6), consistent with features X and A being unresolved for $CrO_3(OCH_3)^-$ (Figure 2). The HOMO-3 to HOMO-5 levels are all predicted to be destabilized from $CrO_3(OH)^-$ to $CrO_3(OCH_3)^-$, in qualitative agreement with the shift of bands C, D, and E to lower binding energy for $CrO_3(OCH_3)^-$ (Tables 1, 2). The calculations indicate that the HOMO-3 and HOMO-4 levels switch order from $CrO_3(OH)^-$ to $CrO_3(OCH_3)^-$, consistent with the position of the weaker shoulder shifting from the low binding energy side of the most intense feature for $CrO_3(OH)^-$ to the high-binding-energy side of this same feature for $CrO_3(OCH_3)^-$. The HOMO-5 is predicted to be destabilized by ~0.6 eV from $CrO_3(OH)^-$ to $CrO_3(OCH_3)^-$, consistent with the shift of band E to about 0.55 eV lower binding energy in the latter. In contrast, the HOMO-6 is shifted much less from $CrO_3(OH)^-$ to $CrO_3(OCH_3)^-$, in agreement with the observation that feature F occurs at a similar binding energy for both species.

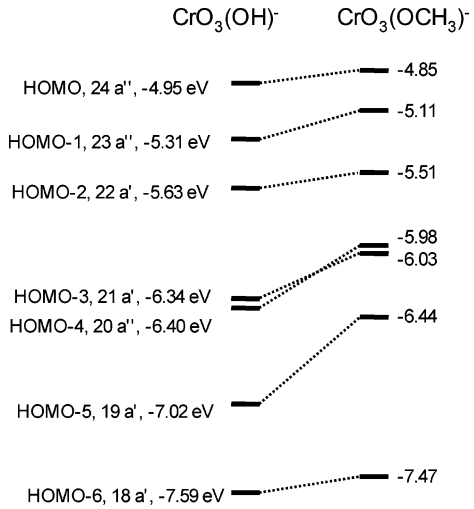

Figure 6. Correlation diagram relating the seven highest-energy occupied orbitals of $CrO_3(OH)^-$ and $CrO_3(OCH_3)^-$. Orbital energies are from the B3LYP calculations and have been shifted for each species to align the energy of the HOMO with the calculated first VDE (see text).

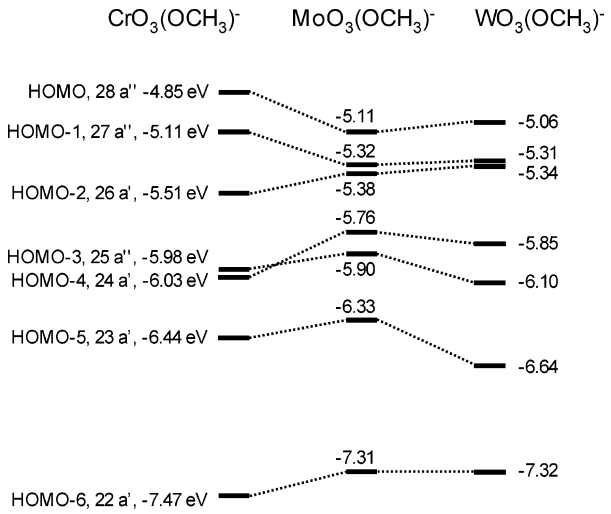

Figure 7. Correlation diagram relating the seven highest-energy occupied orbitals of $MO_3(OCH_3)^-$ (M = Cr, Mo, or W). Orbital energies are from the B3LYP calculations and have been shifted for each species to align the energy of the HOMO with the calculated first VDE (see text).

A correlation diagram relating the predicted energies for the seven highest-energy occupied orbitals of $MO_3(OCH_3)^-$ (M = Cr, Mo, W) is given in Figure 7. The HOMO to HOMO-2 levels of $MoO_3(OCH_3)^-$ and $WO_3(OCH_3)^-$ are predicted to be closer together as compared to the equivalent orbitals of $CrO_3(OCH_3)^-$, in agreement with bands X, A, and B being unresolved for the Mo and W congeners. Equivalent observations were described above for the hydroxo anions. The predicted separation between the HOMO-3 and HOMO-4 levels for $MoO_3(OCH_3)^-$ and $WO_3(OCH_3)^-$ is about 0.14 and 0.25 eV, respectively, much less than that predicted for the equivalent hydroxo anions (~0.5 eV in both cases, Figure 5). This is consistent with the separation between bands C and D for $MoO_3(OH)^-$ and $WO_3(OH)^-$ being about 0.6 eV (Table 1) but much less for the methoxo equivalents (Table 2). The HOMO-5 is predicted to be destabilized by ~0.1 eV from Cr to Mo, but stabilized by ~0.3 eV from Mo to W. This is consistent with the spectral shift of band E to slightly lower binding energy from Cr to Mo, but higher binding energy from Mo to W.

TABLE 5: Calculated Gas-Phase Brønsted Acidities (kcal mol^{-1}) for $MO_2(OR)(OH)$ (M = Cr, Mo, or W; R = H, CH_3, Absent) at the B3LYP and CCSD(T) Levels of Theory[a]

reaction	Cr	Mo	W
$MO_2(OH)_2 \rightarrow MO_3(OH)^- + H^+$	316	317/317	317/317
$MO_2(OCH_3)(OH) \rightarrow MO_3(OCH_3)^- + H^+$	318	319	319
$MO_3(OH) \rightarrow MO_4^- + H^+$	310	310/323	309/315

[a] Values after the "/" are the CCSD(T) values.

The geometries and molecular orbital pictures for $MO_3(OH)^-$ and $MO_3(OCH_3)^-$ provide insight into the changes in orbital energies as a function of metal and ligand. The HOMO to HOMO-7 levels of $MO_3(OR)^-$ are predominantly comprised of oxygen 2p orbitals, suggesting that the relative energies of these orbitals are governed by interactions between these oxo ligands (Figures 4, 5). The Cr−O terminal bond distances in $CrO_3(OH)^-$ (1.60 Å) are significantly shorter than those for $MoO_3(OH)^-$ and $WO_3(OH)^-$ (1.75 and 1.77 Å, respectively; Table 3), resulting in closer contact between oxo ligands for $CrO_3(OH)^-$ (~2.64 Å) as compared with $MoO_3(OH)^-$ and $WO_3(OH)^-$ (~2.84 and 2.88 Å, respectively). This shorter distance results in stronger interactions between oxygen 2p orbitals on these ligands and more significant energetic consequences as a result of these interactions.

The HOMO of $CrO_3(OH)^-$ is best described as an antibonding combination of in-plane oxygen 2p orbitals on the CrO_3 unit (Figure 4). The larger separation between oxo ligands in $MoO_3(OH)^-$ and $WO_3(OH)^-$ results in a reduction in this antibonding interaction and these orbitals being stabilized relative to that of $CrO_3(OH)^-$ (Figure 5). The HOMO-1 involves a π antibonding interaction between O 2p orbitals on two oxo ligands and a π antibonding interaction of an O 2p orbital on the third oxo ligand with an O 2p orbital on the OH ligand. These interactions are again expected to be less repulsive for the Mo and W congeners as a result of the longer M−O bonds in these species, and this orbital is again stabilized for the heavier species (Figure 5). The HOMO-2 involves an O 2p σ bonding interaction between two oxo ligands and a O 2p lone pair on the third oxo ligand. This favorable interaction is increased by the shorter Cr−O bonds in $CrO_3(OH)^-$, and so this orbital is stabilized with respect to the Mo and W congeners (Figure 5). The destabilization of the HOMO and stabilization of the HOMO-2 results in the separation between these levels being much less for $MoO_3(OH)^-$ and $WO_3(OH)^-$ than for $CrO_3(OH)^-$. The HOMO-3 involves a σ bonding interaction between the three terminal oxo ligands, and so is stabilized for $CrO_3(OH)^-$ due to the shorter separation between these ligands. The HOMO-4 orbitals are predominantly O 2p lone pairs on the OH ligand, and the decreasing repulsion of the lone pairs with increasing size leads to a stabilization with increasing atomic number.

The major changes from $CrO_3(OH)^-$ to $CrO_3(OCH_3)^-$ are destabilization of the HOMO-1 and the HOMO-3 to HOMO-5 levels (Figure 6). These orbitals all contain a significant contribution from the methyl moiety (Figure 4). Since the $-OCH_3$ interaction in these three orbitals is antibonding in nature, each of these orbitals is destabilized relative to those of $CrO_3(OH)^-$.

Bond Energies. Heterolytic and homolytic MO−H bond dissociation energies for a variety of mononuclear metal−oxo species were calculated and are presented in Tables 5 and 6, respectively. The energies for the heterolytic cleavage of the O−H bond in $MO_2(OH)_2$ and $MO_2(OH)(OCH_3)$ correspond to the gas-phase acidity at 0 K (proton affinity of the conjugate base anions) and are expected to be accurate to ~1 to 2 kcal/

TABLE 6: Calculated MO−H Bond Dissociation Energies (kcal mol^{-1}) for $MO_2(OR)(OH)$ (M = Cr, Mo, or W; R = H, CH_3, Absent) at the B3LYP and CCSD(T) Levels of Theory[a]

reaction	Cr	Mo	W
$MO_2(OH)(O-H) \rightarrow MO_3(OH) + H$	109	114/118	114/118
$MO_2(OCH_3)(O-H) \rightarrow MO_3(OCH_3) + H$	108	113	113
$MO_3(O-H) \rightarrow MO_4 + H$	93	116/117	116/119
$MO_3(O-H)^- \rightarrow MO_4^- + H$	102	107/124	106/116

[a] Values after the "/" are the CCSD(T) values.

mol on the basis of prior calculations of acidities.[48] The results from the B3LYP and CCSD(T) calculations are in good agreement (Table 5). The calculated acidities of these centers are quite high, being only about 5 to 6 kcal/mol less acidic than H_2SO_4 (acidity = 310.9 kcal/mol) in the gas phase.[48]

The acidities of MO_3OH were also calculated as their conjugate base anions MO_4^- are known in the gas phase.[19,20] The B3LYP and CCSD(T) calculations were in reasonable agreement for $WO_3(OH)$ but in poorer agreement for $MoO_3(OH)$ (Table 5; differences of 6 and 14 kcal mol^{-1}, respectively). Comparison with other calculated values suggested that the CCSD(T) calculations for MoO_4^- are problematic, consistent with the biggest spin contamination and largest T_1 diagnostic[49] for this species. For example, the CCSD(T) ADE for MoO_4^- is 4.67 eV, in poor agreement with an experimental value of 5.20(7) eV.[20] In contrast, the CCSD(T) ADE for WO_4^- is 5.08 eV, in good agreement with the experimental value of 5.1(1) eV.[20]

Homolytic O−H bond dissociation energies (BDE) for a range of mononuclear centers are presented in Table 6. These values are expected to be slightly underestimated on the basis of the fact that only an aug-cc-pVTZ level basis set was used at the CCSD(T) level. The O−H dissociation energy for $MO_2(OCH_3)(OH)$ is similar to that of $MO_2(OH)_2$, consistent with a negligible effect of the methyl group. The first and second BDEs for $MO_2(O-H)_2$ are similar for M = Mo, W, but the second BDE is lower for M = Cr due to the fact that the dissociation product CrO_4 has a different structure with a peroxo ligand bonded to CrO_2 as compared to the two O radical centers in MoO_4 and WO_4.[19,20] Such homolytic MO−H bond dissociation energies can alternatively be estimated from a thermodynamic cycle involving the enthalpy of deprotonation of the parent species (e.g., $MO_2(OH)_2 \rightarrow MO_3OH^- + H^+$, the acidities calculated above; Table 5), the adiabatic electron affinity of the corresponding radical ($MO_3OH^- \rightarrow MO_3OH + e^-$, measured experimentally and calculated above; Tables 1, 4), as well as the ionization potential of H. The values obtained from this cycle for $MO_2(OH)_2$ using the CCSD(T) data are 111, 116, and 119 kcal mol^{-1} for M = Cr, Mo, and W, respectively, and they are in good agreement with the values calculated directly (Table 6). The BDEs for each anion of $MO_2(OR)(OH)$ and $MO_3(OH)$ are comparable and are higher than that of methane and approaching that of H_2O.[50,51] These high O−H dissociation energies suggest that neutral radicals of the form MO_4 or $MO_3(OR)$ should readily abstract H atoms from most organic molecules to initiate catalytic reaction processes, and may be relevant to the catalytic activity of molybdenum and tungsten oxides. On the basis of the reactions of OH radicals, these reactions should occur with modest-to-low barriers dependent on the C−H bond strength.[52−54] The dissociation energy for the anions $MO_3(OH)^-$ to form MO_4^- and H are also high. As described above, differences in the B3LYP and CCSD(T) results for $MoO_3(OH)^-$ are due to the problems with calculating the MoO_4^- species at the CCSD(T) level. The high dissociation energies for $MO_3(OH)^-$ suggested that the anions MO_4^- should be capable of activating many organic molecules in the gas phase, including methane. These anions are readily generated by laser vaporization,[19,20] so this hypothesis could be tested experimentally by mass spectrometry-based experiments.[55,56] For comparison, the related radical cation MoO_3^+ is capable of activating methane and water.[57]

TABLE 7: Calculated Hydroxide, Methoxide, and Fluoride Affinities for MO_3 at the B3LYP and CCSD(T) Level of Theory[a]

	Cr	Mo	W
$MO_3(OH)^- \rightarrow MO_3 + OH^-$	128	138/138	151/151
$MO_3(OCH_3)^- \rightarrow MO_3 + OCH_3^-$	120	130	142
$MO_3F \rightarrow MO_3 + F^-$	122	133	144

[a] Values after the "/" are the CCSD(T) values.

A second dissociation energy relevant to $MO_3(OR)^-$ is loss of an OH^- or OCH_3^- group from the $MO_3(OR)^-$ complex, providing a measure of the Lewis acidity of neutral MO_3 (Table 7). The energies for loss of hydroxide are predicted to increase stepwise from Cr → Mo → W by about 20 kcal/mol in total. Again, for M = Mo and W, the agreement of the B3LYP results with the CCSD(T) results is excellent. Substitution of OCH_3 for OH leads to a lowering of the heterolytic bond energy by about 6 to 10 kcal/mol, consistent with the difference in electron affinities of OH and OCH_3.[58] The high values of these heterolytic bond energies are consistent with the metal centers in MO_3 being extremely strong Lewis acids. Some of us have previously developed a comprehensive Lewis acidity scale based on fluoride affinities.[59] The fluoride affinities of CrO_3, MoO_3, and WO_3 (Table 7) are predicted to be higher than the fluoride affinities of very strong Lewis acids such as SbF_5, again demonstrating the strong Lewis acidity of MO_3.

It is also possible to calculate the homolytic M−OH bond energy in neutral $MO_3(OH)$ to form MO_3 + OH. The bond energies at the B3LYP/aug-cc-pVTZ/ SECP(2f,g) level are 63, 68, and 80 kcal mol^{-1} for M = Cr, Mo, and W, respectively. The CCSD(T)/ aug-cc-pVTZ/SECP(2f,g) bond energies for Mo and W are 64 and 76 kcal/mol, in reasonable agreement with the B3LYP results. These M−OH dissociation energies are substantially lower than those calculated for MO−H (Table 6).

Finally, the hydride affinities for MO_4 were calculated from the reaction $MO_3(OH)^- \rightarrow MO_4 + H^-$. These values are very high with hydride affinities of 179, 207, and 207 kcal mol^{-1} for Cr, Mo, and W, respectively, at the B3LYP/ aug-cc-pVTZ/ SECP(2f,g) level. The CCSD(T)/aug-cc-pVTZ/SECP(2f,g) values of 215 and 217 kcal mol^{-1} for Mo and W, respectively, are about 10 kcal/mol higher than the B3LYP values and support similar hydride affinities for MoO_4 and WO_4.

Conclusions

The electronic structure of the hydroxo and methoxo anions $MO_3(OR)^-$ (M = Cr, Mo, W; R = H, CH_3) were studied experimentally and theoretically by a combination of photoelectron spectroscopy and electronic structure calculations. Systematic comparisons between species with different metals (M = Cr, Mo, W) and ligands (OH, OCH_3) allowed their effect on electronic structure to be elucidated. The comparison between theory and experiment and between the different theoretical methods gave good agreement and indicated that density functional theory can be used to reliably predict the energetics of these Group VI oxo−metal clusters. The experimental and computational data demonstrate the existence of low-energy excited states of neutral $MO_3(OH)$ (e.g., ~0.3 eV for M = Mo, W) in which the radical character localized on an oxygen is shuffled between a MO and MO_2 fragment of $MO_3(OH)$. These

low-energy excited states and resulting changes in electronic and geometric structure might be important in the reactivity and catalytic activity of related molybdenum− and tungsten−oxo sites. The calculations predict high O−H bond dissociation energies for the neutrals $MO_3(OH)$ and $MO_2(OH)_2$ and the anion $MO_3(OH)^-$, suggesting that radicals of the form MO_4, $MO_3(OH)$, and MO_4^-, respectively, should abstract H atoms from many organic molecules to initiate catalytic reaction processes.

Acknowledgment. This work was supported by the Chemical Sciences, Geosciences and Biosciences Division, Office of Basic Energy Sciences, U.S. Department of Energy (DOE) under Grant DE-FG02-03ER15481 (catalysis center program) and was performed at the W. R. Wiley Environmental Molecular Sciences Laboratory, a national scientific user facility sponsored by DOE's Office of Biological and Environmental Research and located at Pacific Northwest National Laboratory, operated for the DOE by Battelle. This work also used the Molecular Sciences Computing Facility in the EMSL at PNNL.

Supporting Information Available: Cartesian coordinates and energies for $MO_2(OR)_2$, $MO_3(OR)^-$, $MO_3(OR)$, and MO_3 (M = Cr, Mo, W; R = H, CH_3) at the different levels of theory described in the text, as well as absolute orbital energies from the B3LYP calculations for each of $MO_3(OR)^-$. This material is available free of charge via the Internet at http:// pubs.acs.org.

References and Notes

(1) *Handbook of Heterogeneous Catalysis*; Ertl, G., Knözinger, H., Weitkamp, J., Eds.; Wiley: Weinheim, Germany, 1997; 2541 pp.

(2) Rao, C. N. R.; Raveau, B. *Transition Metal Oxides*: *Structure, Properties and Synthesis of Ceramic Oxides*, 2nd ed.; Wiley: Weinheim, Germany, 1998; 373 pp.

(3) Jibril, B. Y.; Elbashir, N. O.; Al-Zahrani, S. M.; Abasaeed, A. E. *Chem. Eng. Process.* **2005**, *44*, 835.

(4) Kocon, M.; Michorczyk, P.; Ogonowski, J. *Catal. Lett.* **2005**, *101*, 53.

(5) Ono, Y. *Catal. Today* **2003**, *81*, 3.

(6) Rodriguezramos, I.; Guerreroruiz, A.; Homs, N.; Delapiscina, P. R.; Fierro, J. L. G. *J. Mol. Catal. A* **1995**, *95*, 147.

(7) Yoshinaga, Y.; Kudo, M.; Hasegawa, S.; Okuhara, T. *Appl. Surf. Sci.* **1997**, *121*, 339.

(8) Wang, Y. D.; Chen, Q. L.; Yang, W. M.; Xie, Z. K.; Xu, X.; Huang, D. *Appl. Catal. A* **2003**, *250*, 25.

(9) Soares, A. P. V.; Portela, M. F. *Catal. Rev.*—Sci. Eng. **2005**, *47*, 125.

(10) Zhang, H.; Kou, Y. *Chem. Commun.* **1999**, 1729.

(11) Ohler, N.; Bell, A. T. *J. Catal.* **2005**, *231*, 115.

(12) de Lucas, A.; Valverde, J. L.; Canizares, P.; Rodriguez, L. *Appl. Catal. A* **1999**, *184*, 143.

(13) Wang, H.; Liu, Z. M. *Prog. Chem.* **2004**, *16*, 593.

(14) Plattner, D. A. *Int. J. Mass Spectrom.* **2001**, *207*, 125.

(15) Zemski, K. A.; Justes, D. R.; Castleman, A. W. *J. Phys. Chem. B* **2002**, *106*, 6136.

(16) O'Hair, R. A. J.; Khairallah, G. N. *J. Clust. Sci.* **2004**, *15*, 331.

(17) Bernhardt, T. M. *Int. J. Mass Spectrom.* **2005**, *243*, 1.

(18) Bohme, D. K.; Schwarz, H. *Angew. Chem., Int. Ed.* **2005**, *44*, 2336.

(19) Gutsev, G. L.; Jena, P.; Zhai, H. J.; Wang, L. S. *J. Chem. Phys.* **2001**, *115*, 7935.

(20) Zhai, H. J.; Kiran, B.; Cui, L. F.; Li, X.; Dixon, D. A.; Wang, L. S. *J. Am. Chem. Soc.* **2004**, *126*, 16134.

(21) Zhai, H. J.; Huang, X.; Cui, L. F.; Li, X.; Li, J.; Wang, L. S. *J. Phys. Chem. A* **2005**, *109*, 6019.

(22) Yoder, B. L.; Maze, J. T.; Raghavachari, K.; Jarrold, C. C. *J. Chem. Phys.* **2005**, *122*, 094313.

(23) Haber, J. *Stud. Surf. Sci. Catal.* **1997**, *110*, 1.

(24) Fu, G.; Xu, X.; Lu, X.; Wan, H. L. *J. Am. Chem. Soc.* **2005**, *127*, 3989.

(25) *Biomimetic Oxidations Catalyzed by Transition Metal Complexes*; Meunier, B., Ed.; Imperial College: London, 2000, 696 pp.

(26) Mayer, J. M. *Acc. Chem. Res.* **1998**, *31*, 441.

(27) Yang, X.; Waters, T.; Wang, X. B.; O'Hair, R. A. J.; Wedd, A. G.; Li, J.; Dixon, D. A.; Wang, L. S. *J. Phys. Chem. A* **2004**, *108*, 10089.

(28) Nakayama, H. *Bull. Chem. Soc. Jpn.* **1983**, *56*, 877.

(29) Klemperer, W. G.; Liu, R. S. *Inorg. Chem.* **1980**, *19*, 3863.

(30) Che, T. M.; Day, V. W.; Francesconi, L. C.; Fredrich, M. F.; Klemperer, W. G.; Shum, W. *Inorg. Chem.* **1985**, *24*, 4055.

(31) Wang, L. S.; Ding, C. F.; Wang, X. B.; Barlow, S. E. *Rev. Sci. Instrum.* **1999**, *70*, 1957.

(32) Becke, A. D. *J. Chem. Phys.* **1993**, *98*, 5648.

(33) (a) Aprà, E.; Windus, T. L.; Straatsma, T. P.; Bylaska, E. J.; de Jong, W.; Hirata, S.; Valiev, M.; Hackler, M.; Pollack, L.; Kowalski, K.; Harrison, R.; Dupuis, M.; Smith, D. M. A.; Nieplocha, J.; Tipparaju, V.; Krishnan, M.; Auer, A. A.; Brown, E.; Cisneros, G.; Fann, G.; Früchtl, H.; Garza, J.; Hirao, K.; Kendall, R.; Nichols, J.; Tsemekhman, K.; Wolinski, K.; Anchell, J.; Bernholdt, D.; Borowski, P.; Clark, T.; Clerc, D.; Dachsel, H.; Deegan, M.; Dyall, K.; Elwood, D.; Glendening, E.; Gutowski, M.; Hess, A.; Jaffe, J.; Johnson, B.; Ju, J.; Kobayashi, R.; Kutteh, R.; Lin, Z.; Littlefield, R.; Long, X.; Meng, B.; Nakajima, T.; Niu, S.; Rosing, M.; Sandrone, G.; Stave, M.; Taylor, H.; Thomas, G.; van Lenthe, J.; Wong, A.; Zhang, Z. *NWChem, A Computational Chemistry Package for Parallel Computers, Version 4.6*; Pacific Northwest National Laboratory, Richland, WA 99352-0999, 2004. (b) Kendall, R. A.; Aprà, E.; Bernholdt, D. E.; Bylaska, E. J.; Dupuis, M.; Fann, G. I.; Harrison, R. J.; Ju, J.; Nichols, J. A.; Nieplocha, J.; Straatsma, T. P.; Windus, T. L.; Wong, A. T. *Computer Phys. Comm.*, **2000**, *128*, 260.

(34) Frisch, M. J.; Trucks, G. W.; Schlegel, H. B.; Scuseria, G. E.; Robb, M. A.; Cheeseman, J. R.; Montgomery, J. A., Jr.; Vreven, T.; Kudin, K. N.; Burant, J. C.; Millam, J. M.; Iyengar, S. S.; Tomasi, J.; Barone, V.; Mennucci, B.; Cossi, M.; Scalmani, G.; Rega, N.; Petersson, G. A.; Nakatsuji, H.; Hada, M.; Ehara, M.; Toyota, K.; Fukuda, R.; Hasegawa, J.; Ishida, M.; Nakajima, T.; Honda, Y.; Kitao, O.; Nakai, H.; Klene, M.; Li, X.; Knox, J. E.; Hratchian, H. P.; Cross, J. B.; Bakken, V.; Adamo, C.; Jaramillo, J.; Gomperts, R.; Stratmann, R. E.; Yazyev, O.; Austin, A. J.; Cammi, R.; Pomelli, C.; Ochterski, J. W.; Ayala, P. Y.; Morokuma, K.; Voth, G. A.; Salvador, P.; Dannenberg, J. J.; Zakrzewski, V. G.; Dapprich, S.; Daniels, A. D.; Strain, M. C.; Farkas, O.; Malick, D. K.; Rabuck, A. D.; Raghavachari, K.; Foresman, J. B.; Ortiz, J. V.; Cui, Q.; Baboul, A. G.; Clifford, S.; Cioslowski, J.; Stefanov, B. B.; Liu, G.; Liashenko, A.; Piskorz, P.; Komaromi, I.; Martin, R. L.; Fox, D. J.; Keith, T.; Al-Laham, M. A.; Peng, C. Y.; Nanayakkara, A.; Challacombe, M.; Gill, P. M. W.; Johnson, B.; Chen, W.; Wong, M. W.; Gonzalez, C.; Pople, J. A. Gaussian 03, Revision C.02; Gaussian, Inc.: Wallingford, CT, 2004.

(35) Black, G.; Didier, B.; Elsethagen, T.; Feller, D.; Gracio, D.; Hackler, M.; Havre, S.; Jones, D.; Jurrus, E.; Keller, T.; Lansing, C.; Matsumoto, S.; Palmer, B.; Peterson, M.; Schuchardt, K.; Stephan, E.; Taylor, H.; Thomas, G.; Vorpagel, E.; Windus, T.; Winters, C. , *Ecce, A Problem Solving Environment for Computational Chemistry*, Software Version 3.2.2; Pacific Northwest National Laboratory, Richland, WA 99352-0999, 2005.

(36) Dunning, T. H. *J. Chem. Phys.* **1989**, *90*, 1007.

(37) (a) Dolg, M.; Wedig, U.; Stoll, H.; Preuss, H. *J. Chem. Phys.* **1987**, *86*, 866. (b) Dolg, M. In *Modern Methods and Algorithms of Quantum Chemistry*; Grotendorst, J., Ed.; NIC Series 1; Julich Research Center: Julich, Germany, 2000. (c) Leininger, T.; Berning, A.; Nicklass, A.; Stoll, H.; Werner, H. J.; Flad, H. J. *Chem. Phys.* **1997**, *217*, 19. (d) Kuchle, W.; Dolg, M.; Stoll, H.; Preuss, H. Pseudopotentials of the Stuttgart/Dresden Group, 1998 (Revision: Aug 11, 1998); http://www.theochem.uni-stuttgart.de/pseudopotentiale).

(38) Martin, J. M. L.; Sundermann, A. *J. Chem. Phys.* **2001**, *114*, 3408.

(39) Purvis, G. D. I.; Bartlett, R. J. *J. Chem. Phys.* **1982**, *76*, 1910.

(40) Raghavachari, K.; Trucks, G. W.; Pople, J. A.; Head-Gordon, M. *Chem. Phys. Lett.* **1989**, *157*, 479.

(41) Watts, J. D.; Gauss, J.; Vartlett, R. J. *J. Chem. Phys.* **1993**, 98, 8718.

(42) Werner, H.-J.; Knowles, P. J.; Amos, R. D.; Bernhardsson, A.; Berning, A.; Celani, P.; Cooper, D. L.; Deegan, M. J. O.; Dobbyn, A. J.; Eckert, F.; Hampel, C.; Hetzer, G.; Korona, T.; Lindh, R.; Lloyd, A. W.; McNicholas, S. J.; Manby, F. R.; Meyer, W.; Mura, M. E.; Nicklass, A.; Palmieri, P.; Pitzer, R. M.; Rauhut, G.; Schütz, M.; Stoll, H.; Stone, A. J.; Tarroni, R.; Thorsteinsson, T. MOLPRO-2002, a package of initio programs written by Universität Stüttgart, Stüttgart, Germany, University of Birmingham, Birmingham, U.K., 2002.

(43) (a) Perdew, J. P.; Wang, Y. *Phys. Rev. B* **1991**, *45*, 13244. (b) Burke, K.; Perdew, J. P.; Wang, Y. In *Electronic Density Functional Theory*: *Recent Progress and New Directions*; Dobson, J. F., Ed.; Plenum: New York, 1998. (c) Vignale, G.; Das, M. P.; Perdew, J. P.; Wang, Y. *Phys. Rev. B* **1996**, *54*, 16533.

(44) (a) Garza, J.; Nichols, J. A.; Dixon, D. A. *J. Chem. Phys.* **2000**, *112*, 7880. (b) Garza, J.; Nichols, J. A.; Dixon, D. A. *J. Chem. Phys.* **2000**, *113*, 6029. (c) Garza, J.; Vargas, R.; Nichols, J. A.; Dixon, D. A. *J. Chem. Phys.* **2001**, *114*, 639. (d) Garza, J.; Fahlstrom, C. A.; Vargas, R.; Nichols, J. A.; Dixon, D. A. In *Reviews in Modern Quantum Chemistry: A Celebration of the Contributions of Robert G. Parr*; Sen, K. D., Ed.; World Scientific: Singapore, 2002; Chapter 50, pp 1508−1536. (e) Zhan, C.-G.; Nichols, J. A.; Dixon, D. A. *J. Phys. Chem. A* **2003**, *107*, 4184.

(45) The intensities of the PES bands can be calculated by using time-dependent perturbation theory and the DFT wave function. (Arduengo, A. J., III; Bock, H.; Chen, H.; Denk, M.; Dixon, D. A.; Green, J. C.; Herrmann,

W. A.; Jones, N.; Wagner, M.; West, R. *J. Am. Chem. Soc.* **1994**, *116*, 6641). However, this approximation works best when the photon energy is much higher than the orbital energies, which is not the case here. This method was attempted, but provided poor agreement with experiment and did not aid with an interpretation of the experimental results.

(46) (a) Gassman, P. G.; Mlinaric-Majerski, K.; Kovac, B.; Chen, H.; Dixon, D. A. *J. Phys. Org. Chem.* **1995**, *8*, 14. (b) Stowasser, R.; Hoffmann, *J. Am. Chem. Soc*. **1999**, *121*, 3414.

(47) (a) Reed, A. E.; Curtiss, L. A.; Weinhold, F. *Chem. Rev.* **1988**, *88*, 899. (b) Foster, J. P.; Weinhold, F. *J. Am. Chem. Soc.* **1980**, *102*, 7211. (c) Reed, A. E.; Weinhold, F. *J. Chem. Phys.* **1983**, *78*, 4066. (d) Reed, A. E.; Weinstock, R. B.; Weinhold, F. *J. Chem. Phys.* **1985**, *83*, 735. (e) Reed, A. E.; Weinhold, F. *J. Chem. Phys.* **1985**, *83*, 1736.

(48) Alexeev, Y.; Windus, T. L.; Zhan, C. G.; Dixon, D. A. *Int. J. Quantum Chem.* **2005**, *102*, 775.

(49) Lee, T. J.; Rice, J. E.; Scuseria, G. E.; Schaefer, H. F. *Theor. Chim. Acta* **1989**, *75*, 81.

(50) Ruscic, B.; Wagner, A. F.; Harding, L. B.; Asher, R. L.; Feller, D.; Dixon, D. A.; Peterson, K. A.; Song, Y.; Qian, X. M.; Ng, C. Y.; Liu, J. B.; Chen, W. W. *J. Phys. Chem. A* **2002**, *106*, 2727.

(51) Blanksby, S. J.; Ellison, G. B., *Acc. Chem. Res.* **2003**, *36*, 255.

(52) Atkinson, R. *J. Phys. Chem. Ref. Data, Monograph 2*, **1994**.

(53) Fokin, A. A.; Schreiner, P. R. *Chem. Rev.* **2002,** *102*, 1551.

(54) Sander, S. P.; Friedl, R. R.; Ravishankara, A. R.; Golden, D. M.; Kolb, C. E.; Kurylo, M. J.; Huie, R. E.; Orkin, V. L.; Molina, M. J.; Moortgat, G. K.; Finlayson-Pitts, B. J. Chemical Kinetics and Photochemical Data for Use in Atmospheric Studies: Evaluation Number 14; JPL Publication 02-25, National Aeronautics and Space Administration, Jet Propulsion Laboratory, California Institute of Technology, Pasadena, CA, 2003, http://jpldataeval.jpl.nasa.gov/pdf/JPL_02−25_rev02.pdf.

(55) Schröder, D.; Schwarz, H. *Angew. Chem., Int. Ed. Engl.* **1995**, *34*, 1973.

(56) Schwarz, H.; Schröder, D. *Pure Appl. Chem.* **2000**, *72*, 2319.

(57) Kretzschmar, I.; Fiedler, A.; Harvey, J. N.; Schröder, D.; Schwarz, H. *J. Phys. Chem. A* **1997**, *101*, 6252.

(58) http://webbook.nist.gov/chemistry/.

(59) Christe, K. O.; Dixon, D. A.; McLemore, D.; Wilson, W. W.; Sheehy, J. A.; Boatz, J. A. *J. Fluor. Chem.* **2000**, *101*, 151. See also *Chem. Eng. News* **2003**, *March 3*, pp 48−49.